niques studied the "Wiener" filter is the only one that tries to extract the noise present in the frequency band of interest. Unlike the DFT technique this method does not reject signal content in the higher harmonics. The "Wiener" filter is truly adaptive in that it not only adapts its sampling rate to sample exactly 128 sample points per period of the signal, but also has an adaptive transfer function that changes to give an optimum estimate of the signal derivative in the mean square error sense. While quantitative measures of the performance of the different techniques are difficult to produce in practice, since their performance depends on the signal-to-noise ratio and the amount of overlap between the power density spectra of the signal and the noise, it would be reasonable to suggest, that an accurate differentiator of the left ventricular pressure waveform, which deals optimally with noise both inside and out of the pass band, can be based on the adaptive "Wiener" filter outlined here.

References

[1] A. E. Marble, J. W. Ashe, D. H. K. Tsang, D. Belliveau, and D. N. Swingler, "Assessment of algorithms used to compute the fast Fourier transform of the left ventricular pressure on a microcomputer," *Med. Biol. Eng. Comput.*, vol. 23, pp. 190-194, 1985.

[2] J. Spriet and J. Bens, "Optimal design and comparison of wide-band digital on-line differentiators," *IEEE Trans. Acoust., Speech, Signal Processing*, vol. ASSP-27, pp. 46-52, 1979.

[3] A. Antoniou, "Design of digital differentiator satisfying prescribed specifications," *IEE Proc.*, vol. 127-E, pp. 24-30, 1980.

[4] S. Usui and I. Amidror, "Digital low-pass differentiation for biological signal processing," *IEEE Trans. Biomed. Eng.*, vol. 29, pp. 686-693, 1982.

[5] T. Gasser, W. Kohler, C. Jennen-Steinmetz, and L. Sroka, "The analysis of noisy signals by nonparameteric smoothing and differentiation," *IEEE Trans. Biomed. Eng.*, vol. BME-33, pp. 1129-1133, 1986.

[6] A. E. Marble, C. M. McIntyre, R. Hastings-James, and C. W. Hor, "A comparison of algorithms used in computing the derivative of the left ventricular pressure," *IEEE Trans. Biomed. Eng.*, vol. BME-28, pp. 524-529, 1981.

[7] C. Charayaphan, "An assessment of signal-to-noise ratio of physiological signal using magnitude coherence spectrum," in *Proc. CMBEC*, vol. 13, 1987, pp. 203-204.

[8] G. M. Jenkins and D. G. Watts, *Spectral Analysis and Its Applications*. San Francisco, CA: Holden-Day, 1969.

[9] E. H. Scannell, Jr. and G. Clifford Carter, "Confidence bounds for magnitude-squared coherance estimates," *IEEE Trans. Acoust., Speech, Signal Processing*, vol. ASSP-26, 1978.

Low-Pass Differentiators for Biological Signals with Known Spectra: Application to ECG Signal Processing

PABLO LAGUNA, NITISH V. THAKOR, PERE CAMINAL, AND RAIMON JANÉ

***Abstract*—Digital low-pass filtering and differentiation (LPD) are useful in real-time processing of many biomedical signals. A general method is presented for determining the coefficients of a differentiator that maximizes the signal-to-noise ratio or minimizes the error between actual and ideal LPD filters, when signal and noise spectra are known. Several examples of digital filters suitable for *QRS* complex and *P-T* wave processing in ECG are presented.**

Manuscript received October 27, 1988; revised May 23, 1989. This work was supported by the C.I.R.I.T. Generalitat de Catalunya, Spain, and Grants NS24282 and HL01509 from the National Institute of Health, and Grant 1240/84 from CAICYT, Spain.

P. Laguna, P. Caminal, and R. Jané are with Institut de Cibernética, Universitat Politécnica de Catalunya-CSIC, Barcelona, Spain.

N. V. Thakor is with the Department of Biomedical Engineering, The Johns Hopkins University, School of Medicine, Baltimore, MD 21218.

IEEE Log Number 8933601.

I. Introduction

Biological signals usually have a band-limited spectrum. Signal recordings in practice are corrupted by noise from biological and environmental sources. For example, ECG signal recordings may be corrupted by broad-band muscle noise. Low-pass filters that reject noise frequencies higher than the cutoff frequency of the signal are desirable. Differentiation of biological signal is a useful signal processing tool to extract information about rapid transients in the signal. Low-pass filtering and differentiation are usually implemented in two cascaded stages of digital filters [1], [2]. Some studies have been made to combine these into a single linear filter low-pass differentiator (LPD) [3]-[5].

The current methods do not take into consideration signal and noise spectra. Often signal and noise spectra are known *a priori*, from studies of a large number of experimental recordings [6]. LPD can be optimized from the knowledge of these spectra. Another important consideration is the specific application of our LPD; we may be interested in maximizing the signal-to-noise ratio (SNR) or in preserving the differentiated signal shape while noise content is reduced. We present finite impulse response (FIR) implementations of LPD designed to meet these objectives. We present theoretical criteria for determining the best LPD coefficients and give the values obtained for: 1) *QRS* detection in noise, 2) *P*, *T* waves detection in noise, 3) *P*, *T* waves enhancement with respect to *QRS*.

II. Theory

We employ the notation of [3] where the ideal LPD frequency response is given by (Fig. 1)

$$H(a, \omega) = \begin{cases} j\omega & |\omega| \le a\pi \\ 0 & a\pi < |\omega| \le \pi \end{cases} \tag{1}$$

where $a\pi$, $(0 < a \le 1)$, denotes the upper limit of the differentiation band and j is the complex imaginary unit. For the sake of simplicity, we assume the sampling interval to be equal to one unit of time ($T = 1$). Let f_s be the sampling rate and f_c^* be the cutoff frequency of the LPD, so that

$$a = 2\frac{f_c^*}{f_s}. \tag{2}$$

The ideal filter in its most general form is

$$H(a, \omega) = \sum_{n=-\infty}^{\infty} C'_{n_s} \exp(jn\omega). \tag{3a}$$

Alternately, a different base $\exp(j(n - 1/2)\omega)$ leads to

$$H(a, \omega) = \sum_{n=-\infty}^{\infty} C'_{n_a} \exp\left(j(n - 1/2)\omega\right) \tag{3b}$$

where C'_{n_s} and C'_{n_a} are the coefficients of the ideal filter, which have an implicit dependence of parameter a.

The approximate FIR filter obtained with N finite number of coefficients can be expressed as

$$F_s(\omega) = j \sum_{n=1}^{N} C_{n_s} \sin(n\omega) \tag{4a}$$

$$F_a(\omega) = j \sum_{n=1}^{N} C_{n_a} \sin\left((n - 1/2)\omega\right) \tag{4b}$$

where C_{n_s}, C_{n_a} are the coefficients of the filter approximation.

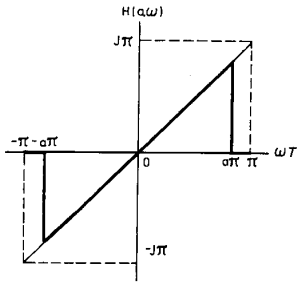

Fig. 1. Ideal low-pass-differentiator (LPD) transfer function for a cutoff parameter a, $(0 < a < 1)$.

We call these two filter forms F_s and F_a, symmetric and asymmetric, respectively. For sampled data, the time-domain expressions for these filters are

$$Y_s(k) = d/2 \sum_{n=1}^{N} \overline{C}_{n_s}(X(k+n) - X(k-n)) \quad \text{with } d\,\overline{C}_{n_s} = C_{n_s} \tag{5a}$$

$$Y_a(k) = d/2 \sum_{n=1}^{N} \overline{C}_{n_a}(X(k+n) - X(k-n+1)) \quad \text{with } d\,\overline{C}_{n_a} = C_{n_a} \tag{5b}$$

where d is a scale factor that results in integer values for $\overline{C}_{n_s}$, $\overline{C}_{n_a}$; $Y_s(k)$, $Y_a(k)$ are the filter outputs at sample time k, and $X(k)$ is the sampled input at time k. Note that Y_a is delayed by $1/2$ sample interval. In future derivations we will use the notation F, Y and coefficients C_n for both the symmetric and the asymmetric forms. These two bases are needed to cover all directly implementable FIR LPD.

A. LPD with Reduced Mean-Squared Error

Assume that the signal has a spectrum $S(\omega)$ with a cutoff frequency f_c and sampling rate f_s. Let noise have spectrum $N(\omega)$ if it is known *a priori* from experimental work. The output of the ideal differentiator will be $j\omega S(\omega)$. In order to obtain a real differentiator output $S(\omega)\,F(\omega)$ as a good replica of the ideal output, we must make the difference between the ideal $H(a, \omega)$ and the real $F(\omega)$ small, especially at frequencies where $\omega S(\omega)$ is high.

Under these considerations, we define the square-error $E(a)$ as follows:

$$E(a) = \int_{-\pi}^{\pi} \left|H(a, w) - F(\omega)\right|^2 W(\omega)\, d\omega \tag{6}$$

with the weight factor $W(\omega)$ defined as

$$W(\omega) = \begin{cases} \omega S(\omega)/S0 & |\omega| < a\pi \\ N(\omega)/N0 & a\pi < |\omega| < \pi \end{cases} \tag{7}$$

with

$$S0 = \int_{-a\pi}^{a\pi} \omega S(\omega)\, d\omega$$

and

$$N0 = \int_{-\pi}^{-a\pi} N(\omega)\, d\omega + \int_{a\pi}^{\pi} N(\omega)\, d\omega. \tag{8}$$

Then we define the best real coefficients $(C_1, C_2, \cdots, C_N)$ as those that minimize $E(a)$. This definition leads to the following relation:

$$\int_{-a\pi}^{a\pi} W(\omega)\, d\omega = \int_{-\pi}^{-a\pi} W(\omega)\, d\omega + \int_{a\pi}^{\pi} W(\omega)\, d\omega. \tag{9}$$

It ensures that the error between 0 and $a\pi$, and between $a\pi$ and π receives the same importance. This is important since usually we have $(a < 1/2)$ to avoid aliasing problems, and without this distribution of weights we could make a precise approximation of the low-pass part of the filter, and a rather poor one of the differentiation.

Usually the spectrum of the signal $S(\omega)$ is a continuous but complex function of ω. In order to simplify the calculations, we approximate $S(\omega)$ by a function with r linear parts, and then obtain an analytical second-order expression for $E(a)$. From (6) we obtain $E(a)$ as a function of filter coefficients, their squared values and parameter a.

$$E(a) = E(a, C_1, C_2, \cdots, C_N, C_1^2, C_2^2, \cdots, C_N^2). \tag{10}$$

As we can see in [3] minimization of (10) does not imply that the error for low frequencies is minimum. Therefore, we minimize (10) with an additional restriction of ideal behavior at $\omega = 0$.

$$\left.\frac{dF(\omega)}{d\omega}\right|_{\omega=0} = j.$$

Then from (4), we require that

$$\sum_{n=1}^{N} nC_{n_s} = 1, \qquad \sum_{n=1}^{N} (n - 1/2)C_{n_a} = 1 \tag{11}$$

and we can write

$$C_N = C_N(C_1, C_2, \cdots, C_{(N-1)}). \tag{12}$$

Combining (10) and (12)

$$E(a) = E(a, C_1, C_2, \cdots, C_{(N-1)}, C_1^2, \cdots, C_{(N-1)}^2). \tag{13}$$

To minimize this expression we must solve a linear system of $N-1$ equations with $N-1$ unknowns.

$$\frac{dE(a)}{dC_i} = E_i(a, C_1, \cdots, C_{(N-1)} = 0 \quad \text{for } i = 1, \cdots, N-1. \tag{14}$$

From (14) and (11) we obtain a set of N coefficients that minimize $E(a)$.

B. LPD for Signal-to-Noise Ratio (SNR) Improvement

In the above study we do not consider noise in the signal spectrum, but sometimes the spectrum is contaminated with noise that we cannot remove without distorting the signal. In these cases we design an LPD that optimizes SNR. With this criterion the filter may not reproduce the signal accurately, but may be useful for some applications (like *QRS* detection) where we need a good SNR. First we define

$$\mathrm{SNR1}(a) = \frac{\int_{-\pi}^{\pi} S(\omega)\, H(a, \omega)\, d\omega}{\int_{-\pi}^{\pi} N(\omega)\, H(a, \omega)\, d\omega}. \tag{15}$$

SNR1 is calculated from ideal differentiator $H(a, \omega)$. Since SNR1 is a function of a, we can maximize (15) and obtain the best $a = a_0$ (and from (2) we get cutoff frequency f_c^*) that maximizes SNR1.

On the other hand, SNR2 is the real SNR obtained with actual filter $F(\omega)$.

$$\mathrm{SNR2} = \frac{\int_{-\pi}^{\pi} \left|S(\omega)\, F(\omega)\right|^2 d\omega}{\int_{-\pi}^{\pi} \left|N(\omega)\, F(\omega)\right|^2 d\omega}. \tag{16}$$

Note that (16) is quadratic because $F(\omega)$ can be both positive and negative in the range $(0 < \omega < \pi)$. The function in (16) must be

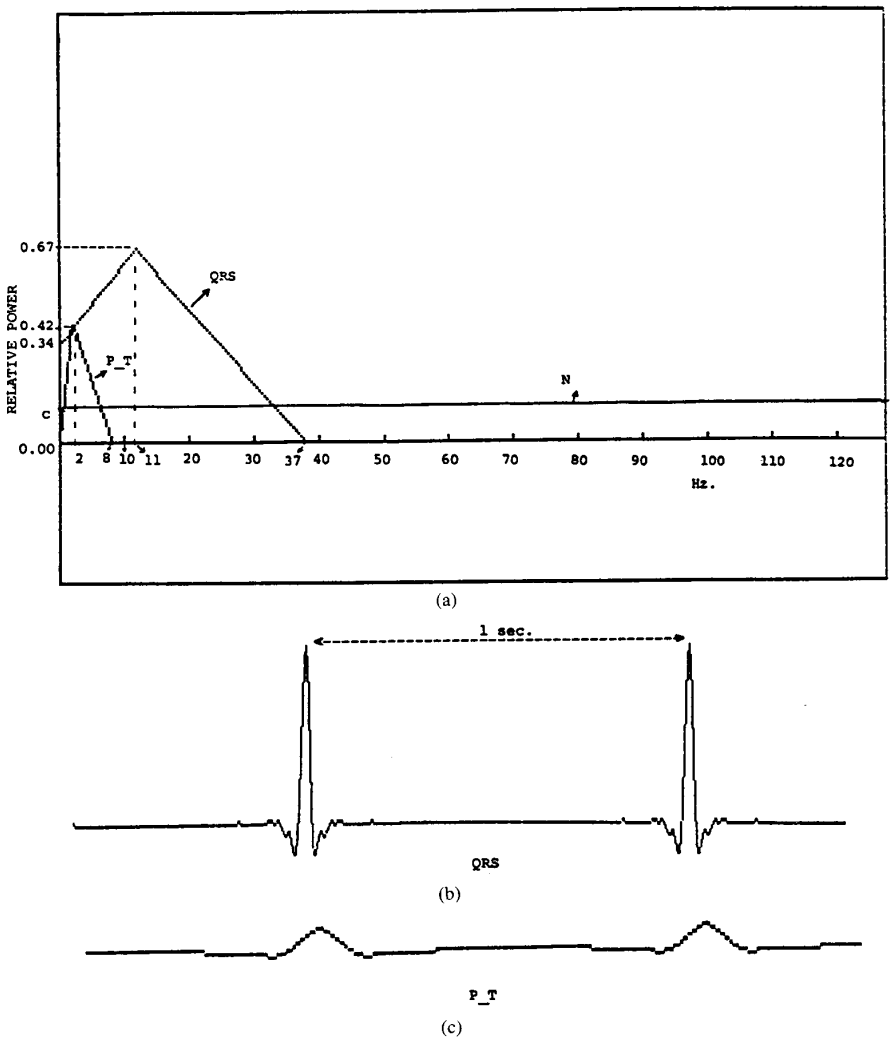

Fig. 2. (a) Linear approximation of the *QRS* complex and *P*, *T* waves spectra in two parts: for *QRS* in ($f = 0, f_1 = 11$) Hz and ($f_1 = 11, f_c = 37$) Hz; for *P-T* in ($f = 0, f_1 = 2$) Hz and ($f_1 = 2, f_c = 8$) Hz. This is an approximation of spectra given by [6]. (b) *QRS* signal recovered from spectra in Fig. 2(a) under restriction explained in text, sampling rate of 250 Hz and 1 s of periodicity. (c) *P*, *T* waves recovered from spectra in (a) with the same conditions than in (b).

maximized with respect to filter coefficients C_i ($i = 1, \cdots, N-1$), but this requires solution of a third-order system of $N-1$ equations with $N-1$ unknowns which is difficult to do analytically. Therefore, we take a_0 from (15), minimize $E(a_0)$ in (13), and obtain the best C_n as in (14). Finally, as described below, we find the nearest integer approximation to the coefficients C_n that maximizes SNR2.

C. Filter Coefficient Approximation

With the above described criteria we find the best set of N coefficients to be $C_1, C_2, \cdots, C_N$. But these may not always be desirable. In general, minimization with sufficiently large number of coefficients $_P$ results in higher values of C_n for some n. Thus, when all coefficients $C_1, \cdots, C_P$ are examined, a few selected coefficients $C_{r_1}, C_{r_2}, \cdots, C_{r_N}$ may be the largest. A filter can be constructed with minimization of $E(a)$ from only these largest coefficients without a significant loss in performance. It would also be advisable to examine $E(a)$ for adjacent filter coefficients $C_{(r_1 \pm 1)}, C_{(r_2 \pm 1)}, \cdots, C_{(r_N \pm 1)}$.

Another approximation is to convert real value coefficients to normalized integer value coefficients ($\bar{C}_n$) in order to improve the computational speed. Since such quantization and normalization modify the error $E(a)$, it is advised to consider adjacent coefficient values also.

III. Applications

We illustrate the methods mentioned above with applications to ECG signal processing in three different situations: 1) *QRS* detection in noise, 2) *P*, *T* waves detection in noise, and 3) *P*, *T* waves enhancement with respect to *QRS* complexes.

We take a linear approximation of the *QRS* and *P-T* spectra given in [6] and approximated in Fig. 2(a), in two parts: for frequencies in $(0, f_1)$ and (f_1, f_c), which from (2) correspond to ω in $(0, a_1\pi)$ and $(a_1\pi, a\pi)$.

$$S(\omega) = \begin{cases} r_1 \quad \omega + p_1 & |\omega| < a_1\pi \\ r_2 \quad \omega + p_2 & a_1\pi < |\omega| < a\,\pi \\ 0 & a\pi < |\omega| < \pi \end{cases} \tag{17}$$

From spectra in Fig. 2(a) and sampling rate of $f_s = 250$ Hz. ($T = 4$ ms), for $QRS(\omega)$ spectrum

$$f_1 = 11 \text{ Hz} \quad f_c = 37 \text{ Hz}$$

and from (2)

$$a_1 = 0.088 \quad a = 0.296 \quad r_1 = 1.114$$

$$p_1 = 0.34 \quad r_2 = -1.036 \quad p_2 = 0.97.$$

for $PT(\omega)$ spectrum

$$f_1 = 2 \text{ Hz} \quad f_c = 8 \text{ Hz}$$

and from (2)

$$a_1 = 0.016 \quad a = 0.064 \quad r_1 = 8.355$$

$$p_1 = 0.00 \quad r_2 = -2.785 \quad p_2 = 0.56.$$

If the ideal signal is assumed to be symmetric then the signal shape can be recovered from the spectra in Fig. 2(a). Fig. 2(b) shows the morphology of the ideal *QRS* and Fig. 2(c) *P*, *T* waveforms recovered from the approximated spectra in Fig. 2(a).

A. QRS Detection in Noise

If we are interested in *QRS* detection we must improve signal to noise ratio at the LPD filter output; then we proceed as explained in Section II-B. Assuming that noise comes basically from muscle sources, we may suppose white noise [6]. We find that the ideal a which maximizes (15) corresponds to a cutoff frequency $f_c^* = 14.9$ Hz. Then we minimize $E(a)$ with $H(a)$ corresponding to this cutoff frequency, and find the nearest integer coefficients that maximize (16).

Let c be the power spectral density for $N(\omega)$, and *QRS-D*1, *QRS-D*2, *QRS-D*3 be the optimum filters (in sense of Section II-B) with 1, 2, and 3 coefficients respectively for *QRS* detection. Subindexes (a, s) denote symmetric or asymmetric configuration, respectively. We obtain

	d	$(\bar{C}_1, \bar{C}_2, \bar{C}_3)_{s,a}$	SNR2 c^2
*QRS-D*1:	1/2	$(0, 1, 0)_s$	0.374;
*QRS-D*2:	1/38.5	$(0, 9, 10)_a$	0.655;
*QRS-D*3:	1/43	$(4, 6, 7)_s$	0.800;

SNR2 c^2 increases with number of coefficients, thus improving performance for *QRS* detection in presence of noise. Also, if c (noise power spectrum) decreases SNR2 increases.

Fig. 3(a) shows transfer functions ($QRS\text{-}Di(\omega)$ $i = 1, 2, 3$; $QRS(\omega)$; and ideal LPD) and Fig. 3(b) *QRS-Di* filter outputs for a real ECG with added white noise. An improvement of performance is evident when the number of coefficients increases.

B. P, T Waves Detection in Noise

P, *T* waves detection problem is similar to the *QRS* detection problem; this implies taking $S(\omega) = P\_T(\omega)$. Maximizing SNR1 in (15) we obtain the ideal a corresponding to cutoff frequency $f_c^* = 3.19$ Hz. Minimizing $E(a)$ and rounding coefficients to maximize SNR2 we get the filter coefficients. The filters for 1, 2, 3 coefficients are

	d	$(\bar{C}_9, \bar{C}_{10}, \bar{C}_{11}, \bar{C}_{12})_{s,a}$	SNR2 c^2
*PT-D*1:	1/11.5	$(0, 0, 0, 1)_a$	0.012
*PT-D*2:	1/21	$(0, 1, 1, 0)_s$	0.023
*PT-D*3:	1/31.5	$(0, 1, 1, 1)_a$	0.035.

The SNR improves when the number of coefficients increases. For the same noise power, the SNR2 is lower than in *QRS* detection; this is as a result of lower signal power for *P*, *T* waves as compared with *QRS*.

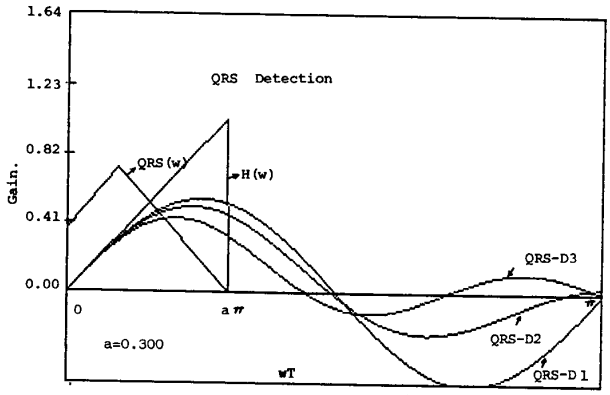

(a)

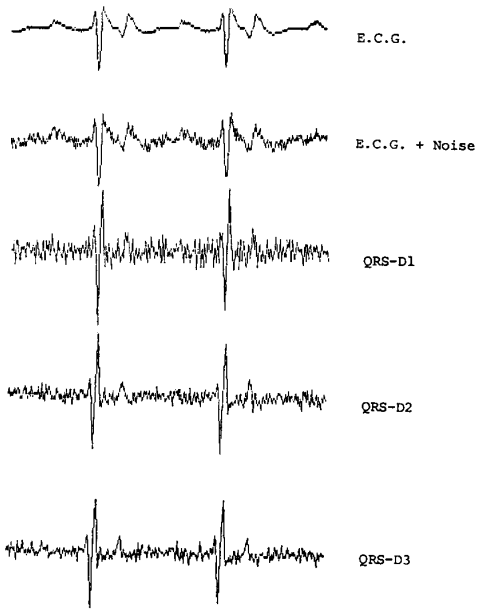

(b)

Fig. 3. (a) Transfer functions for: $QRS\text{-}Di(\omega)$ ($i = 1, 2, 3$) filters, $QRS(\omega)$ spectrum, and ideal LPD for *QRS* wave. (b) Results on an ECG signal: original ECG, ECG with added white noise, with SNR $a = 10$ $\left(\text{SNR } a = \dfrac{\text{maximum signal amplitude}}{\text{maximum noise amplitude}}\right)$, and outputs of *QRS-Di* from noisy signal.

Fig. 4(a) shows the transfer functions for $PT\text{-}Di(\omega)$, $P\_T(\omega)$, and ideal LPD. Fig. 4(b) shows *PT-Di* filter outputs for the same real ECG, with added white noise. Note how in this case *P* and *T* waves are proportionally more magnified than *QRS* wave.

C. P, T Waves Enhancement with Respect to QRS

In order to extract *P*, *T* waves from ECG we consider *QRS* as noise, and try to maximize SNR; operating as for *QRS*, *P_T* detection but now with $N(\omega) = QRS(\omega)$; $S(\omega) = P\_T(\omega)$ we found that the best a which maximizes SNR1 corresponds to a frequency $f_c = 2.875$ Hz. When $E(a)$ is minimized, considering *QRS* as noise in $W(\omega)$, and doing the integer approximation we obtain the fol-

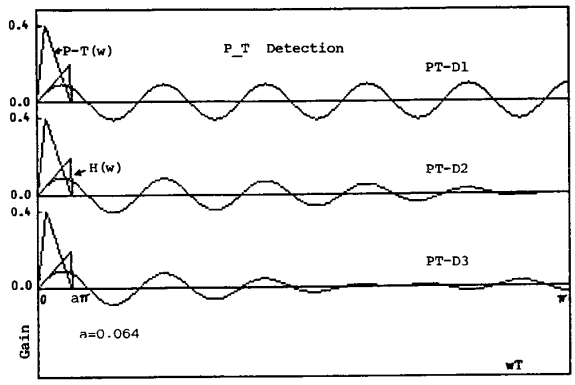

(a)

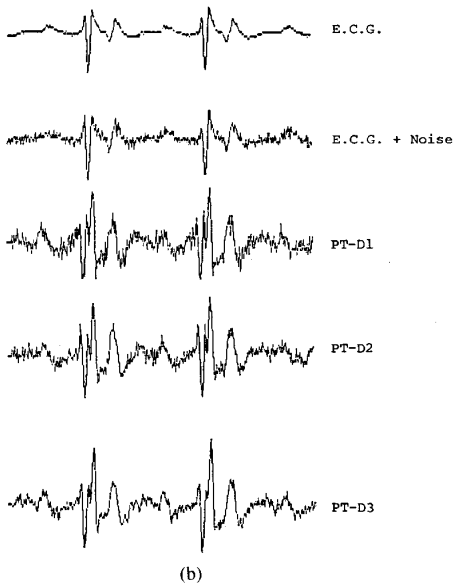

(b)

Fig. 4. (a) Transfer functions for: $PT\text{-}Di(\omega)$ $(i = 1, 2, 3)$ filters, $P\_T(\omega)$ spectrum, and ideal LPD for P, T waves. (b) Results on an ECG signal: original ECG, ECG with added white noise, with SNR $a = 10$ as defined in Fig. 3, and outputs of $PT\text{-}Di$ from noisy signal.

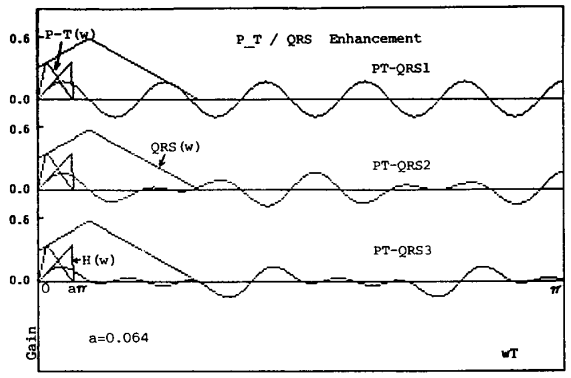

(a)

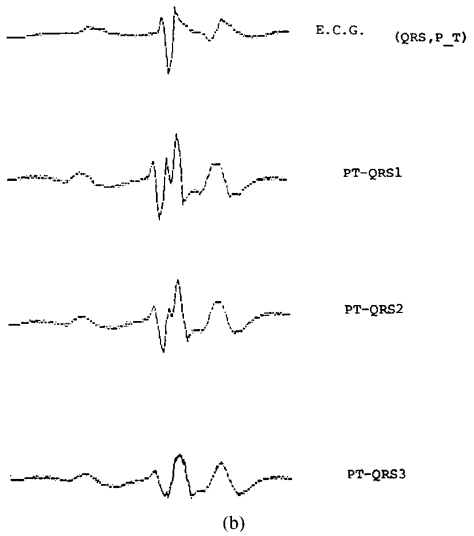

(b)

Fig. 5. (a) Transfer functions for: $PT\text{-}QRSi(\omega)$ $(i = 1, 2, 3)$ filters, $P\_T(\omega)$, and $QRS(\omega)$ spectra, and ideal LPD for P, T waves. (b) Results on an ECG signal: original ECG, and outputs of $PT\text{-}QRSi$ from original signal.

lowing $PT\text{-}QRSi$, $(i = 1, 2, 3)$ optimum filters, with 1, 2, and 3 coefficients, respectively.

	d		SNR2
$PT\text{-}QRS1$:	1/10.5	$(\overline{C}_{11} = 1)_a$	0.0547
$PT\text{-}QRS2$:	1/21	$(\overline{C}_9 = 1, \overline{C}_{13} = 1)_a$	0.219
$PT\text{-}QRS3$:	1/30	$(\overline{C}_5 = 1, \overline{C}_{10} = 1, \overline{C}_{15} = 1)_s$	0.347.

(21)

Here we have an exact value of SNR2 hence we know the relative noise power with respect to signal $(QRS(\omega), P\_T(\omega))$.

Fig. 5(a) shows the transfer functions for $PT\text{-}QRSi(\omega)$ $(i = 1, 2, 3)$, $P\_T(\omega)$, $QRS(\omega)$ (this now must be seen as noise) and ideal LPD for P, T waves. Note that the gain is low between cutoff frequency of $P\_T(\omega)$ and cutoff frequency of $QRS(\omega)$ as we desired, and after these values $PT\text{-}QRSi(\omega)$ can take any value, since neither signal nor noise are supposed to be present beyond the cutoff frequency.

Fig. 5(b) shows $PT\text{-}QRSi$ filter outputs from a real ECG signal in the three cases considered where we see a bigger PT/QRS relation as number of coefficients increases, and better than in original signal.

Table I presents these results for sampling rates $f_s = 200$, 250, and 300 Hz, three very common sampling rates in ECG signal processing. We can see how as we increase f_s, order of filter coefficients increases. That is evident if we believe that higher sampling rate leads to an increase in the number of samples, and therefore the coefficient order, to get same calculations.

IV. Conclusions

We present a general method to derive FIR LPD for digital processing of ECG signals. This method assumes *a priori* knowledge of both signal and noise spectra. This may not always be possible in general applications, but in biological signals we usually know an estimate of the spectra of signals such as ECG, as well as noise sources such as EMG. This knowledge can be applied to theoretical design of the filter. The derived LPD filters are time invariant, then they may introduce some distortion of the signal when its spectrum changes significantly from the time-invariant estimate. We apply this technique to ECG signal processing for three common sampling rates. The method can be generalized to other signals and other sampling rates. For example, an important application is in

TABLE I
OPTIMUM LPD FOR ECG SIGNAL PROCESSING AT SAMPLING RATES f_s = 200, 250, 300 Hz IN THE THREE CASES CONSIDERED IN TEXT. (NORMALIZATION FACTOR d VALUE CAN BE CALCULATED FROM EQUATIONS (11a, b) AND (5)

QRS Detection		$d(\overline{C}_1, \overline{C}_2, \overline{C}_3, \overline{C}_4)_{s,a}$		
		f_s = 200 Hz	f_s = 250 Hz	f_s = 300 Hz
	*QRS-D*1:	$1/1.5\ (0, 1, 0, 0)_a$	$1/2\ (0, 1, 0, 0)_s$	$1/2.5\ (0, 0, 1, 0)_a$
	*QRS-D*2:	$1/21.5\ (0, 6, 5, 0)_a$	$1/38.5\ (0, 9, 10, 0)_a$	$1/5\ (0, 1, 1, 0)_s$
	*QRS-D*3:	$1/43\ (8, 10, 5, 0)_s$	$1/37\ (4, 6, 7, 0)_s$	$1/82\ (0, 8, 10, 9)_a$
PT Detection				
		f_s = 200 Hz $d(\overline{C}_7, \overline{C}_8, \overline{C}_9, \overline{C}_{10})_{s,a}$	f_s = 250 Hz $d(\overline{C}_9, \overline{C}_{10}, \overline{C}_{11}, \overline{C}_{12})_{s,a}$	f_s = 300 Hz $d(\overline{C}_{11}, \overline{C}_{12}, \overline{C}_{13}, \overline{C}_{14})_{s,a}$
	*PT-D*1:	$1/8\ (0, 1, 0, 0)_s$	$1/11.5\ (0, 0, 0, 1)_a$	$1/12.5\ (0, 0, 1, 0)_a$
	*PT-D*2:	$1/16\ (0, 1, 1, 0)_a$	$1/21\ (0, 1, 1, 0)_s$	$1/24\ (0, 1, 1, 0)_s$
	*PT-D*3:	$1/24\ (1, 1, 1, 0)_s$	$1/31.5\ (0, 1, 1, 1)_a$	$1/37.5\ (0, 1, 1, 1)_a$
PT/QRS Enhancement			$d(\overline{C}_i, \overline{C}_j, \cdots)$	
		f_s = 200 Hz	f_s = 250 Hz	f_s = 300 Hz
	*PT-QRS*1:	$1/8.5\ (\overline{C}_9 = 1)_a$	$1/10.5\ (\overline{C}_{11} = 1)_a$	$1/13\ (\overline{C}_{13} = 1)_s$
	*PT-QRS*2:	$1/17\ (\overline{C}_7 = 1, \overline{C}_{11} = 1)_a$	$1/21\ (\overline{C}_9 = 1, \overline{C}_{13} = 1)_a$	$1/25\ (\overline{C}_{10} = 1, \overline{C}_{15} = 1)_s$
	*PT-QRS*3:	$1/24\ (\overline{C}_4 = 1, \overline{C}_8 = 1, \overline{C}_{12} = 1)_s$	$1/30\ (\overline{C}_5 = 1, \overline{C}_{10} = 1, \overline{C}_{15} = 1)_s$	$1/36\ (\overline{C}_6 = 1, \overline{C}_{12} = 1, \overline{C}_{18} = 1)_s$

neurophysiologic work where neural spike signals are recorded by microelectrodes and must be discriminated from the background noise of the brain. An LPD filter may be employed here to detect neural spikes in real time.

REFERENCES

[1] J. Pan and W. J. Tompkins, "A real-time *QRS* detection algorithm," *IEEE Trans. Biomed. Eng.*, vol. BME-32, pp. 230–236, Mar. 1985.

[2] O. Pahlm and L. Sornmo, "Software *QRS* detection in ambulatory monitoring—A review," *Med. Biol. Eng. Comput.*, vol. 22, pp. 289–297, 1984.

[3] U. Shiro and A. Itzhak, "Digital low-pass differentiation for biological signal processing," *IEEE Trans. Biomed. Eng.*, vol. BME-29, pp. 686–693, Oct. 1982.

[4] B. Andrews and D. Jones, "A note of the differentiation of human kinematic data," in *Dig. 11th Int. Conf. Med. Biol. Eng.*, Ottawa, Ont., Canada, 1976, pp. 88–89.

[5] M. D. Lesh, J. M. Mansour, and S. R. Simon, "A gait analysis subsystem for smoothing and differentiation of human motion data," *J. Biomed. Eng.*, vol. 101, pp. 203–212, 1979.

[6] N. V. Thakor, J. G. Webster, and W. J. Tompkins, "Estimation of *QRS* Complex Power Spectra for Design of a *QRS* Filter," *IEEE Trans. Biomed. Eng.*, vol. BME-31, pp. 702–706, Nov. 1984.

A Perfused Tissue Phantom for Ultrasound Hyperthermia

P. J. BENKESER, L. A. FRIZZELL, K. R. HOLMES, AND S. A. GOSS

***Abstract*—A perfused tissue phantom, developed as a tool for analyzing the performance of ultrasound hyperthermia applicators, was investigated. The phantom, consisting of a fixed porcine kidney with thermocouples placed throughout the tissue, was perfused with degassed water by a variable flow rate pump. The phantom was insonated by an unfocused multielement ultrasound applicator and the temperatures in the phantom were recorded. The results indicate that for testing protocols where tissue phantoms are needed, the fixed kidney preparation offers an opportunity to use a more realistic phantom than has previously been available to assess the heating performance of ultrasound hyperthermia applicators.**

Manuscript received November 21, 1988; revised August 11, 1989. This work was supported in part by Labthermics Technologies, Inc., NIH Training Grant CA09067, and Grant NIH -HL27011.

P. J. Benkeser is with the School of Electrical Engineering, Georgia Institute of Technology, Atlanta, GA 30332.

L. A. Frizzell is with the Bioacoustics Research Laboratory, Department of Electrical and Computer Engineering, University of Illinois, Urbana, IL 61801.

K. R. Holmes is with the Department of Veterinary Bioscience and Bioengineering Faculty, University of Illinois, Urbana, IL 61801.

S. A. Goss is with Labthermics Technologies, Inc., Champaign, IL 61820.

IEEE Log Number 8933602.

I. INTRODUCTION

The goal of hyperthermic treatment of a tumor is to elevate the temperature of its entire volume to the therapeutic range, typically 43–45°C. Perfusion plays an important role in shaping the temperature distribution in tissues heated with hyperthermia applicators, and can vary significantly during the course of a given treatment [1]–[3]. To experimentally evaluate the performance of an applicator in a treatment simulation, a perfused tissue phantom must be employed in order to obtain realistic temperature distributions.

Due to the complex blood perfusion patterns present in normal tissue and tumors, it is difficult to construct a phantom to simulate these patterns [4]. Several simple dynamic phantoms have been constructed for microwave hyperthermia purposes [5], [6]. The flow geometry through these phantoms is quite different from that in tissue. Because of this difference, the temperature distributions obtained with these phantoms possess a questionable relationship to actual patient temperatures [4]. The use of dog kidneys and thigh muscles as *in vivo* thermal models have been reported by several researchers [7], [8]. However, the experimental complexity associated with these *in vivo* models makes them impractical as a simple and repeatable system for assessing the heating capabilities of a particular applicator design.

The purpose of the present work is to determine if a recently developed perfused tissue phantom can serve as a simple and easy to maintain device for analyzing more realistically the heating capabilities of ultrasound hyperthermia applicators.

II. METHODS AND MATERIALS

A. Perfused Tissue Phantom

The perfused tissue phantom employed in this study was an alcohol-fixed porcine kidney. This preparation possesses a system of perfusion channels whose structure closely resembles that of the